The Madden-Julian oscillation detected in Aquarius salinity observations

Gary Grunseich,[1] Bulusu Subrahmanyam,[2] and Bin Wang[1]

Received 29 September 2013; revised 10 October 2013; accepted 11 October 2013.

[1] The Madden-Julian Oscillation (MJO) impacts a wide range of weather and climate phenomena. Current global coupled ocean-atmospheric general circulation models exhibit considerable shortcomings in representing and predicting the MJO, specifically its initiation, due to a lack of in situ observations. Here we show, for the first time, that the MJO propagation can be detected from the newly launched NASA Aquarius Salinity mission. The magnitude and extent of sea surface salinity (SSS) variations during the MJO is established, providing a useful tool for data assimilation into models to correctly represent both oceanic and atmospheric processes during intraseasonal variations. Salinity observation allows for atmospheric conditions to be inferred from freshwater flux, on which surface salinity is highly dependent. Increased observations of global SSS from the Aquarius mission will be particularly valuable in remote regions of the tropics and will increase our dynamical understanding and advance prediction of the MJO through model improvement.
Citation: Grunseich, G., B. Subrahmanyam, and B. Wang (2013), The Madden-Julian oscillation detected in Aquarius salinity observations, *Geophys. Res. Lett.*, *40*, doi:10.1002/2013GL058173.

1. Introduction

[2] On the intraseasonal scale, the dominant mode of climate variability known as the Madden-Julian Oscillation (MJO) [*Madden and Julian*, 1971] affects the tropics through strong air-sea coupling [*Wang and Xie*, 1998; *Fu et al*., 2003] and influences many global meteorological phenomena [*Bond and Vecchi*, 2003; *Matthews*, 2004; *Maloney and Hartmann*, 2000]. The convective anomalies propagate eastward at an average speed of 5 ms^{-1} and typically cover 12,000–20,000 km of the equatorial belt [*Rui and Wang*, 1990]. The mechanisms that produce the MJO breakdown into two hypotheses: (1) The MJO is a response to a pre-existing forcing, and (2) the MJO is sustained by its own energy source through coupled circulation patterns; therefore, accurate initial conditions are vitally important for intraseasonal prediction [*Fu et al*., 2011]. With the increasing availability of satellite and in situ observations, the dynamics of the MJO will be better understood and the dynamic prediction will improve.

[3] The launch of the United State's NASA and Space Agency of Argentina's (Comisión Nacional de Actividades Espaciales) Aquarius/Satelite de Aplicaciones Cientificas (SAC)-D satellite mission on 10 June 2011 created new opportunities in addressing research questions regarding the variability of salinity and ocean dynamics. The fundamental objectives of Aquarius are to enhance our knowledge of ocean circulation, climate variability, land processes, land use, soil moisture, and the hydrological cycle [*Le Vine et al*., 2007; *Lagerloef et al*., 2012]. The mission retrieves salinity measurements from the brightness temperature (T_B) of the sea surface, which is measured with an L-band radiometer (1.4 GHz frequency). To acquire the sea surface salinity (SSS) measurement, algorithms are used to correct for surface roughness (a function of wind, waves, and rain), atmospheric gases, sea surface temperature, Faraday rotation, and solar and galactic emission sources, which collectively attenuate the brightness temperature. Unlike the Soil Moisture and Ocean Salinity mission, an onboard scatterometer is used to take simultaneous measurements of surface roughness directly along the swath [*Le Vine et al*., 2007; *Camps et al*., 2005; *Font et al*., 2004]. The Aquarius swath is 390 km wide [*Lagerloef et al*., 2008] formed with a three beam push broom configuration (76×94, 84×120, and 96×156 km), with a repeat time of 7 days, equating to approximately four samples per month at a given location.

[4] SSS responds to freshwater flux (precipitation minus evaporation) and wind-driven advection, making it an ideal variable to utilize when understanding the response of the ocean to atmospheric processes during the MJO [*Matthews et al*., 2010; *Grunseich et al*., 2011]. Positive SSS anomalies are produced during periods of enhanced winds and clear skies (positive Outgoing Longwave Radiation (OLR) anomalies), which increase evaporation. Enhanced precipitation and cloud cover (negative OLR anomalies), combined with a reduction in winds, lead to a reduction in salinity anomalies. Additionally, advection can produce salinity anomalies, especially in tropical regions of the Indian Ocean where the horizontal salinity gradients are strong.

[5] Besides being a variable that responds passively to atmospheric conditions, SSS significantly controls upper ocean density and therefore the Mixed Layer Depth (MLD). The formation of a Barrier Layer, the layer between the MLD and Isothermal Layer Depth, can lead to possible feedbacks that impact the atmospheric component of the MJO, as stated as one of the three major hypotheses of the Dynamics of the Madden-Julian Oscillation (DYNAMO) field campaign. This layer produces a stable stratification, reducing vertical mixing, which influences surface heat fluxes and thus could possibly impact atmospheric conditions during the MJO. Establishing the magnitude and extent of SSS variations during the MJO will be a useful tool for data assimilation into models to correctly represent both oceanic thermodynamic characteristics and atmospheric processes during intraseasonal variations.

[1]Department of Meteorology, School of Ocean and Earth Science and Technology, University of Hawai'i at Mānoa, Honolulu, Hawaii, USA.
[2]Marine Science Program and Department of Earth and Ocean Sciences, University of South Carolina, Columbia, South Carolina, USA.

Corresponding author: G. Grunseich, Department of Meteorology, School of Ocean and Earth Science and Technology, University of Hawai'i at Mānoa, Honolulu, HA 96822, USA. (ggruns@hawaii.edu)

0094-8276/13/10.1002/2013GL058173

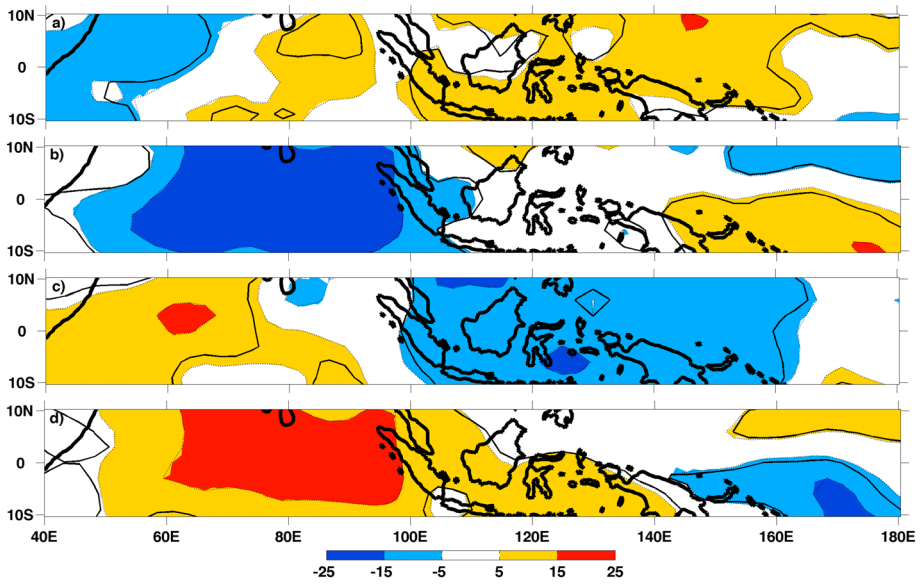

Figure 1. Composites of OLR anomalies (W/m^2) during different stages of the MJO propagation. Composite dates are based on peak negative OLR anomalies arriving at (a) 60°E and (b) 90°E. Dates of subsequent peak positive OLR anomalies at (c) 60°E and (d) 90°E are composited to complete an entire convective propagation. Statistically significant anomalies at the 90% level are indicated with solid contours.

[6] In this study, we show for the first time the SSS variations measured from the Aquarius salinity mission that occur during the MJO and identify the mechanisms that produce the fluctuations. Accurate quantification of sea surface salinity during the MJO will lead to the improvement of models, data assimilation, dynamical prediction, and, most importantly, MJO initialization.

2. Data and Methods

[7] To delineate the impact of the MJO on SSS, the phases of MJO propagation during the Aquarius mission were determined. A technique similar to *Rui and Wang* [1990] was used to identify different stages of the MJO propagation in the Indian and Western Pacific Oceans. NOAA interpolated Outgoing Longwave Radiation (OLR) data [*Liebmann and Smith*, 1996] from 2 September 2011 to 18 February 2013 were averaged into a 7 day temporal resolution to match the Aquarius salinity measurements and were filtered using a ninth order Butterworth band-pass filter, which isolated the 30–80 day signal. Hovmoller diagrams of filtered OLR centered on the equator were constructed to identify different phases of the MJO propagation. By requiring negative OLR anomalies to propagate greater than 100° of longitude and maintain anomalies $\leq -5\ W\ m^{-2}$, a total of 10 strong MJO-related convective phases, or event-bands, was identified. Composite analysis, using OLR anomalies produced by removing the annual mean, was completed based on the dates when the MJO-associated minimum OLR anomalies crossed 60°E and 90°E as well as when the subsequent maximum OLR anomalies crossed these longitudes. Statistical significance was computed using a Student's *t* test for each grid point. Taken together, these composites (Figure 1) show the propagation of convective anomalies (negative OLR anomalies) from the western Indian Ocean to the central Pacific Ocean over the 30–80 day cycle.

[8] We used Aquarius/SAC-D version 2.0 Level 3, weekly gridded (1° × 1°) sea surface salinity data, from the NASA Jet Propulsion Laboratory (JPL) Physical Oceanography Distributed Active Archive Center (PO.DAAC), to isolate the MJO SSS signal in the tropical oceans for the September 2011 to February 2013 period. To produce the Level 3 gridded maps, the quality flags were applied to remove pixels with possible radio frequency interference contamination, as well as extract only the highest quality SSS values based on the radiometer and scatterometer flags. The three beams, based on the highest quality, were then combined to produce a single SSS value on a 1° × 1° global grid [*Lagerloef*, 2013]. The satellite-derived SSS fluctuations during the different stages of the MJO propagation were identified using the same event dates and longitudinal locations that were used to form MJO composites of the OLR data. Composites were smoothed using a Gaussian filter with a 3 × 3 grid point kernel. Daily 0.25° × 0.25° gridded, merged Tropical Rainfall Measuring Mission (TRMM) and other satellites rainfall estimates (3B42 V6 derived) from Goddard Earth Sciences Data and Information Services Center [*Huffman et al.*, 2007, 2010] as well as daily 1° × 1° evaporation measurements from the Woods Hole Oceanographic Institution (WHOI) Objectively Analyzed air-sea Fluxes (OAFlux) project were useful in identifying the mechanisms that produce these SSS anomalies. The daily TRMM rainfall rate and evaporation data were averaged to a 7 day temporal resolution to match the same periods covered by the Aquarius SSS data.

3. Results

[9] MJO-related convective anomalies initially form over the western Indian Ocean while suppressed convection persists throughout the maritime continent and western Pacific (Figure 1a). The MJO-related convection intensifies, expands, and propagates to the central Indian Ocean while the inactive phase propagates further to the east (Figure 1b).

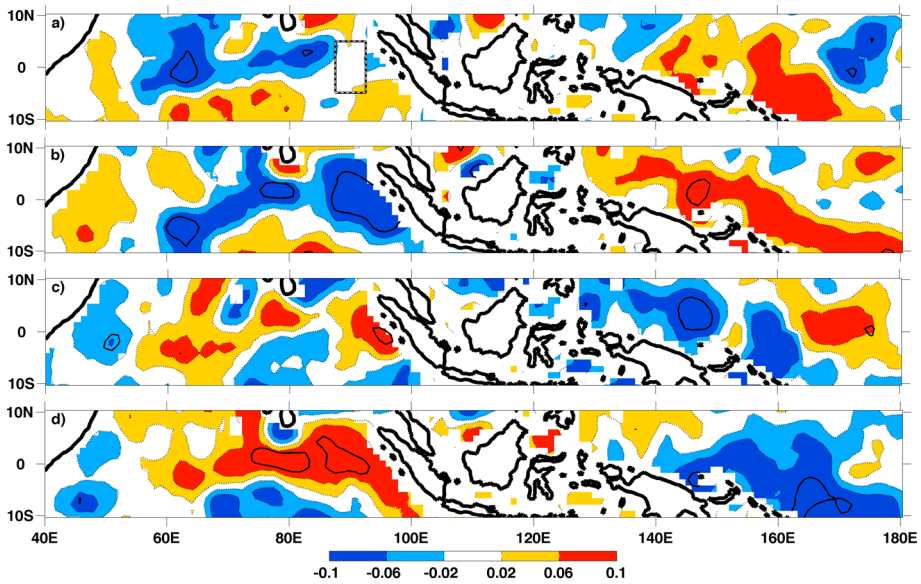

Figure 2. Composites of SSS anomalies during different stages of the MJO propagation. Composites are produced using the same event dates identified to create Figure 1. Statistically significant anomalies at the 90% level are indicated with solid contours. (a) The box represents the region where spatial averages are taken (5°S to 5°N, 87.5°E to 92.5°E).

The next composite shows the propagation of convection over the maritime continent and into the western Pacific Ocean as well as the development of the inhibited convective stage of the MJO in the western Indian Ocean (Figure 1c). The final composite reveals the dissipation of convective anomalies in the western Pacific Ocean and the intensification of positive OLR anomalies in the central to eastern Indian Ocean (Figure 1d).

[10] The SSS composites, when compared with the OLR composites, reveal a strong relationship between the atmospheric conditions and SSS response. When the convective anomalies develop in the western Indian Ocean, an area of negative SSS anomalies is also produced in this region, while positive SSS anomalies in the western Pacific coincide with the suppressed convective MJO phase (Figure 2a). When the convective (negative OLR) anomalies peak in the eastern Indian Ocean, negative SSS anomalies grow in spatial extent as well as amplitude (Figure 2b). In the Western Pacific, positive SSS anomalies also increase in extent and amplitude following the inactive phase of the MJO in this region (Figure 2b). Once the MJO-related convective anomalies arrive over the maritime continent and western Pacific, negative SSS anomalies are produced in this region while a small area of positive SSS anomalies between 160°E and 180°E still lingers (Figure 2c). Additionally, the development of positive OLR anomalies in the western Indian Ocean coincides with positive SSS anomaly formation in this region (Figure 2c). In the final composite, the dissipating phase of the convective anomalies in the western Pacific Ocean corresponds to strong and extensive negative SSS anomalies (Figure 2d). During the same time period, this inactive convective phase of the MJO peaks in the eastern Indian Ocean, producing a broad area of positive SSS anomalies from the central Indian Ocean to the Sumatran coast. Throughout the tropical Indian and Pacific Oceans, SSS fluctuations remain largely statistically insignificant, although a discernable pattern appears in the composites. This is likely due to only 10 cases being considered as well as no composite analysis based on season, due to the short time span of the Aquarius data. *Grunseich et al.* [2011] demonstrated using Simple Ocean Data Assimilation reanalysis that as the propagation of the MJO shifts seasonally, the SSS anomalies in the Indian Ocean fluctuate as well.

[11] Composite analysis shows that there is a clear SSS signal produced during the various stages of the MJO propagation. Hovmoller diagrams of filtered OLR (Figure 3a), Precipitation minus Evaporation (P minus E) (Figure 3b), and filtered Aquarius SSS (Figure 3c) from 60°E to 180°E and averaged over 5°S to 5°N demonstrate the relationship between atmospheric conditions during 10 MJO propagations of convective anomalies and the consequent SSS response. During all 10 identified convectively active periods, P minus E typically increases to over 6 mm/d (Figure 3b) and corresponds well with the negative OLR anomalies (Figure 3a). During all 10 active MJO periods, negative SSS anomalies of at least −0.1 are produced (Figure 3c). The SSS anomalies form in the central Indian Ocean and propagate eastward at the same speed as the OLR anomalies and resemble the high P minus E pattern. During the strongest MJO events (e.g., February 2012), the SSS anomalies propagate to roughly 170°E. During periods of MJO-suppressed convective anomalies (Figure 3a), regions of low positive P minus E values are observed throughout the longitudinal band, with negative values occurring over the eastern Indian Ocean and Maritime Continent (Figure 3b). Throughout the entire time period, the relative importance of precipitation verses evaporation in the equatorial Indian and Pacific Oceans can be observed. Precipitation largely dominates this region with light precipitation falling even during the positive OLR anomaly periods. Figure 3b demonstrates that the tropical Indian and Pacific Oceans exhibit high precipitation rates, but on an intraseasonal timescale, it is highly variable. The reduction in rain rate enhances P minus E and produces positive SSS anomalies (Figure 3c). The positive SSS anomalies occur during the peak in OLR anomalies and the minimum in P minus E in the central

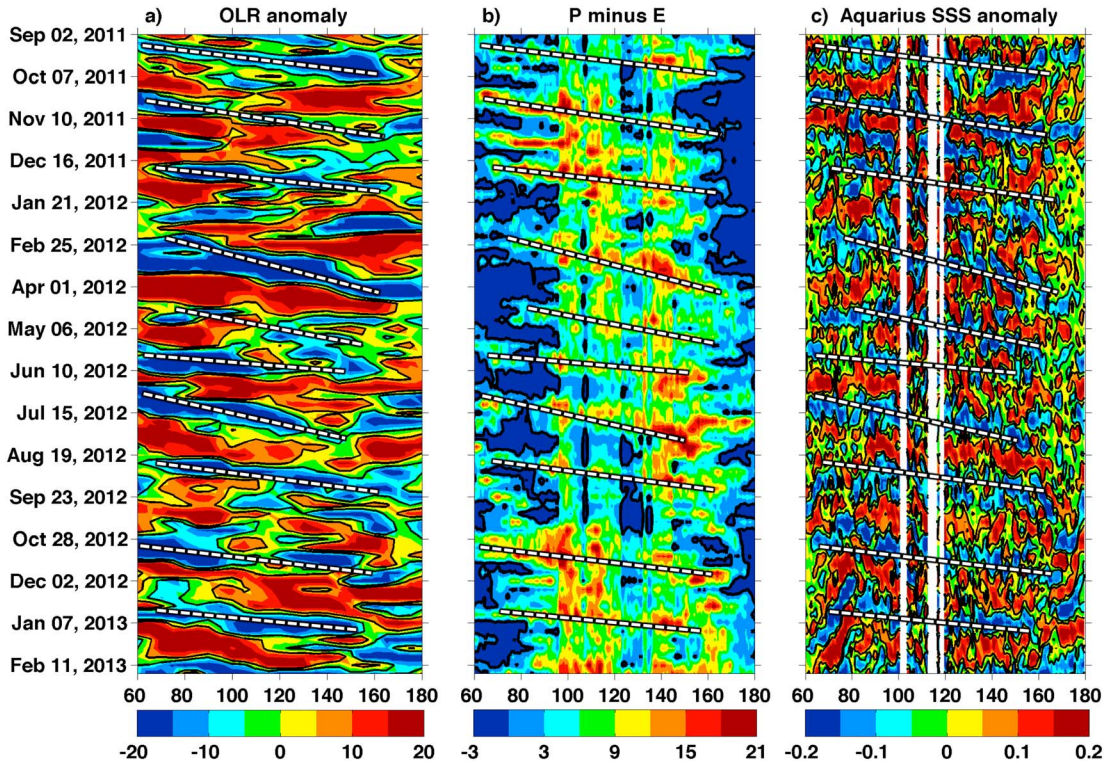

Figure 3. Hovmoller diagrams of (a) filtered OLR (W/m^2), (b) TRMM rain rate (mm/d), and (c) filtered Aquarius SSS. Data are averaged over 5°S to 5°N for each longitudinal point. Dashed white lines mark the 10 convective phases of the MJO that were identified during this time period.

Indian Ocean and follow the propagation of positive OLR anomalies into the western Pacific Ocean.

[12] To understand the relationship between OLR, P minus E, and SSS in greater detail, time series were constructed for all four data sets and averaged over 5°S–5°N, 87.5°E–92.5°E (shown in Figure 2a). This location was chosen because it is a site of strong, persistent MJO-related activity, even during seasonal fluctuations in the direction of propagation, before weakening over the maritime continent [*Rui and Wang*, 1990; *Zhu and Wang*, 1993; *Wang et al.*, 2006]. A connection between the variables can be distinguished with periods of negative OLR anomalies (Figure 4a) corresponding to high P minus E (Figure 4b) and reduced SSS (Figure 4c) during times of strong MJO activity. In general, the production of MJO-related negative SSS anomalies corresponds well with P minus E values of over 5 mm/d. Periods of positive OLR anomalies (Figure 4a) correspond to a reduction in P minus E (Figure 4b), typically near or below 0 mm/d, and

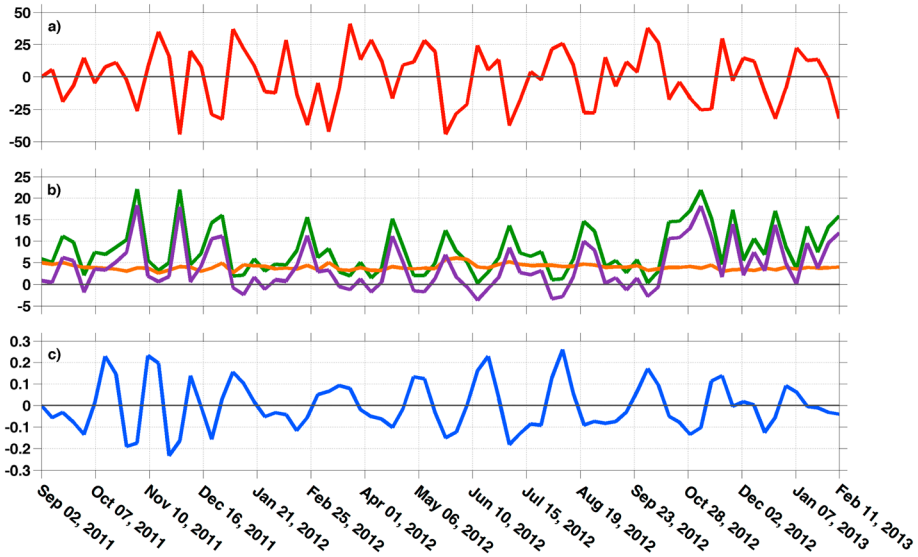

Figure 4. Time series of (a) filtered OLR (W/m^2), (b) precipitation (green), evaporation (orange), and precipitation minus evaporation (purple) (mm/d), and (c) filtered Aquarius SSS averaged over 5°S to 5°N, 87.5°E to 92.5°E (shown in Figure 2a).

an increase in SSS (Figure 4c). The relative importance of precipitation over evaporation is highlighted in this region with precipitation rates generally far exceeding evaporation rates except during times of positive OLR anomalies (Figure 4b). At zero lag, correlations between P minus E and filtered SSS reach an r value of -0.49 while between filtered OLR and SSS, an r value of 0.54 is attained. In early 2012, a period of minimal MJO-related activity occurs, producing irregular OLR and precipitation fluctuations, which likely lower the correlations of SSS with OLR and P minus E. In the latter half of 2012, an increase in P minus E is displayed, which could be due to the seasonal shift in propagation direction of the MJO, which becomes eastward (as opposed to northeastward during the boreal summer) [*Zhang and Dong*, 2004], allowing for stronger convection to pass over the region as activity becomes centered on the equator. The close relationship between the four variables shows the important role of precipitation during the active MJO phase and evaporation during the suppressed convection phase and the nearly immediate production of SSS anomalies.

4. Discussion

[13] The atmospheric conditions associated with varying phases of the MJO propagation are responsible for the development of SSS anomalies. This study examines the magnitude and extent of salinity variations at the surface during the MJO using satellite-derived data. Previous studies such as *Matthews et al*. [2010] utilize Argo observations to explain how the MJO modulates salinity. Unlike Aquarius, which measures salinity directly at the surface, Argo measurements are taken from 5 to 10 m depth (10 dbar). When compared with our results, SSS anomalies during the development of the convective phase appear to be less pronounced in the Argo data. This is possibly due to the weak atmospheric forcing that exists during this phase having little impact on the depth where the observations are taken. When the convection is strongest in the Eastern Indian Ocean, our results are consistent in showing the production of negative salinity anomalies, but in the western Pacific Ocean, Argo data show contrasting negative salinity anomalies. During the production of positive OLR anomalies in the Indian Ocean, both studies show positive salinity anomalies, but in the western Pacific Ocean, dissimilar results appear. These comparisons indicate that salinity variability during the MJO in the Western Pacific Ocean requires additional study in the future.

[14] In remote locations where key atmospheric variables such as precipitation and evaporation are difficult to detect, SSS can act as a proxy to infer the local atmospheric conditions. Additionally, accurate SSS measurements during different stages of the MJO propagation could prove useful in understanding the dynamics behind the MJO. During various phases of the MJO, SSS is controlled by evaporation, precipitation, and advection [*Grunseich et al*., 2011; *Matthews et al*., 2010]. The importance of upper ocean features such as the mixed layer has been highlighted in *Wang and Xie* [1998], who showed that the mixed layer provides an energy source for amplifying atmospheric Kelvin waves, favors the development of unstable planetary-scale modes, and significantly reduces the eastward propagation speed of Kelvin waves to match the MJO timescale. Recently, attention has been given to an upper ocean feature known as the Barrier Layer, which has been shown to impact meteorological phenomena from El Niño–Southern Oscillation [*Maes et al*., 2005] to tropical cyclones [*Balaguru et al*., 2012]. The barrier layer is formed due to a thin mixed layer in the presence of salinity stratification, which suppresses vertical mixing and thereby helps to reduce sea surface cooling through enhanced surface heat fluxes. The calculation in *Sprintall and Tomczak* [1992] defines the barrier layer as the difference between the isothermal layer depth and mixed layer depth. The isothermal layer depth is defined as the depth in which temperature changes 0.2°C from the surface value while the mixed layer depth is the depth in which potential density, a function of salinity, increases with respect to the surface by a density difference equivalent to a temperature decrease of 0.2°C. Proper representation of these features relies on precise observations of SSS, subsurface salinity, and temperature to attain accurate measurements of the mixed layer depth and subsequently the barrier layer thickness. Compared to the many available in situ SSS measurements, Aquarius currently obtains the closest observations to the true sea surface. The pairing of in situ subsurface salinity and temperature measurements with Aquarius observations will allow for the role of near-surface features to be better understood.

[15] The ability of Aquarius to accurately detect the variations in SSS during different stages of the MJO propagation shows that it will be a useful tool in understanding MJO dynamics. The MJO-related sea surface salinity variations have only been shown in model simulations [*Grunseich et al*., 2011] and satellite studies utilizing additional oceanic parameters to understand the dynamics are only beginning [*Grunseich and Subrahmanyam*, 2013]. Analysis of SSS simulations from Hybrid Coordinate Ocean Model output revealed that high-resolution ocean general circulation models exhibit difficulty in producing the same magnitude, spatial, and temporal variations in SSS during MJO propagations when compared with Aquarius data. This affirms that Aquarius-derived SSS will be a useful tool for data assimilation, model advancement, improvement of initialization, and better representation of both oceanic and atmospheric processes during intraseasonal variations. Accurate SSS observations collected by the Aquarius salinity mission at the current spatial coverage and duration are unprecedented. It has now been shown that the measurements gathered from this mission will broaden our understanding in various modes of climate variability even on intraseasonal scales.

[16] **Acknowledgments.** Gary Grunseich and Bin Wang are supported by NOAA MAPP and ESS projects. Bulusu Subrahmanyam is supported by the NASA Physical Oceanography Program award NNX13AM60G. Aquarius version 2.0 data were provided by NASA/JPL PO.DAAC. The authors would like to thank the Aquarius team for providing the Level 3 Ocean Salinity data, WHOI OAFlux project for providing evaporation data, and two anonymous reviewers for their assistance in evaluating the paper.

[17] The Editor thanks two anonymous reviewers for their assistance in evaluating this paper.

References

Balaguru, K., P. Chang, R. Saravanan, L. R. Leung, Z. Xu, M. Li, and J. S. Hsieh (2012), Ocean barrier layers' effect on tropical cyclone intensification, *Proc. Natl. Acad. Sci. U. S. A.*, *109*, 14,343–14,347.

Bond, N. A., and G. A. Vecchi (2003), The influence of the Madden-Julian Oscillation on precipitation in Oregon and Washington, *Weather Forecast.*, *18*, 600–613.

Camps, A., M. Vall-Illopsserra, L. Batres, F. Torres, N. Duffo, and I. Corbella (2005), Retrieving sea surface salinity multiangular L-band brightness temperature: Improvement by spatiotemporal averaging, *Radio Sci.*, *40*, RS2003, doi:10.1029/2004RS003040.

Font, J., G. Lagerloef, and D. Le Vine (2004), The determination of surface salinity with the European SMOS space mission, *IEEE Trans. Geosci. Remote Sens.*, *42*, 2196–2205.

Fu, X., B. Wang, T. Li, and J. P. McCreary (2003), Coupling between northward-propagating, intraseasonal oscillations and sea surface temperature in the Indian Ocean, *J. Atmos. Sci.*, *60*, 1733–1753.

Fu, X., B. Wang, J.-Y. Lee, W. Wang, and L. Gao (2011), Sensitivity of dynamical intra-seasonal prediction skills to different initial conditions, *Mon. Weather Rev.*, *139*, 2572–2592.

Grunseich, G., and B. Subrahmanyam (2013), Detection of the Madden-Julian oscillation in the Indian Ocean from satellite altimetry, *IEEE Geosci. Remote Sens. Lett.*, *10*, 441–445.

Grunseich, G., B. Subrahmanyam, and A. Arguez (2011), Influence of the Madden-Julian oscillation on sea surface salinity in the Indian Ocean, *Geophys. Res. Lett.*, *38*, L17605, doi:10.1029/2011GL049047.

Huffman, G. J., R. F. Adler, D. T. Bolvin, G. Gu, E. J. Nelkin, K. P. Bowman, Y. Hong, E. F. Stocker, and D. B. Wolff (2007), The TRMM multi-satellite precipitation analysis: Quasi-global, multi-year, combined-sensor precipitation estimates at fine scale, *J. Hydrometeorol.*, *8*, 38–55.

Huffman, G. J., R. F. Adler, D. T. Bolvin, and E. J. Nelkin (2010), The TRMM multi-satellite precipitation analysis (TMPA), in *Satellite Rainfall Applications for Surface Hydrology*, edited by F. Hossain, and M. Gebremichael, chap. 1, pp. 3–22, Springer Verlag Düsseldorf, Germany.

Lagerloef, G. (2013), Aquarius salinity validation analysis, Aquarius Project Document: AQ-014-PS-0016, 18 February 2013, Data Version 2.0.

Lagerloef, G. E., et al. (2008), The Aquarius/SAC-D mission: Special issue on salinity, *Oceanography*, *21*, 69–81.

Lagerloef, G., F. Wentz, S. Yueh, H. Kao, G. Johnson, and J. Lyman (2012), Aquarius satellite mission provides new, detailed view of sea surface salinity, [in "*State of the Climate in 2011*"], *Bull. Am. Meteorol. Soc.*, *93*, S70–S71.

Le Vine, D. M., G. S. E. Lagerloef, R. Colomb, S. Yueh, and F. Pellerano (2007), Aquarius: An instrument to monitor sea surface salinity from space, *IEEE Trans. Geosci. Remote Sens.*, *45*, 2040–2050.

Liebmann, B., and C. A. Smith (1996), Description of a complete (interpolated) outgoing longwave radiation dataset, *Bull. Am. Meteorol. Soc.*, *77*, 1275–1277.

Madden, R. A., and P. R. Julian (1971), Detection of a 40–50 day oscillation in the zonal wind in the tropical Pacific, *J. Atmos. Sci.*, *28*, 702–708.

Maes, C., J. Picault, and S. Belamari (2005), Importance of salinity barrier layer for the buildup of El Niño, *J. Clim.*, *18*, 104–108.

Maloney, E. D., and D. L. Hartmann (2000), Modulation of eastern North Pacific hurricanes by the Madden-Julian oscillation, *J. Clim.*, *13*, 1451–1460.

Matthews, A. J. (2004), Intraseasonal variability over tropical Africa during northern summer, *J. Clim.*, *17*, 2427–2440.

Matthews, A. J., P. Singhruck, and K. J. Heywood (2010), Ocean temperature and salinity components of the Madden-Julian oscillation observed by Argo floats, *Clim. Dyn.*, *35*, 1149–1168.

Rui, H., and B. Wang (1990), Development characteristics and dynamic structure of tropical intraseasonal convection anomalies, *J. Atmos. Sci.*, *47*, 357–379.

Sprintall, J., and M. Tomczak (1992), Evidence of the barrier layer in the surface layer of the tropics, *J. Geophys. Res.*, *97*, 7305–7316.

Wang, B., and X. Xie (1998), Coupled modes of the warm pool climate system. Part I: The role of air-sea interaction in maintaining Madden-Julian Oscillation, *J. Clim.*, *8*, 2116–2135.

Wang, B., P. Webster, K. Kikuchi, T. Yasunari, and Y. Qi (2006), Boreal summer quasi-monthly oscillation in the global tropics, *Clim. Dyn.*, *27*, 661–675.

Zhang, C., and M. Dong (2004), Seasonality of the Madden Julian oscillation, *J. Clim.*, *15*, 2429–2445.

Zhu, B., and B. Wang (1993), The 30–60 day convection seesaw between the tropical Indian and western Pacific Oceans, *J. Atmos. Sci.*, *50*, 184–199.